Special Section: UZIG USGS
Vadose Zone Journal

Water Movement through a Shallow Vadose Zone: A Field Irrigation Experiment

Carlos G. Ochoa,* Alexander G. Fernald, Steven J. Guldan, and Manoj K. Shukla

Surface irrigation water percolating below the crop rooting zone is important for groundwater recharge in agricultural areas overlying shallow aquifers. The objective of this study was to characterize water movement through the shallow vadose zone following surface irrigation. Two infiltration plots were installed in each of three predominant local soil types. Plots were instrumented to measure soil water content and shallow groundwater level. Data were used to calculate water infiltration, velocity of propagation of the wetting front, water fluxes, and water level response following irrigation. Results showed a low to moderate infiltration rate (0.001–0.056 m h^{-1}), relatively low levels of propagation of the wetting front (0.13–0.79 m h^{-1}), water flux (0.001–0.13 m h^{-1}), and shallow groundwater response (0.01–0.1 m) in Fruitland sandy loam and Werlog clay loam soils. In the Abiquiu-Peralta soil, however, a higher infiltration rate (0.002–0.124 m h^{-1}), wetting front propagation (0.28–3.75 m h^{-1}), water flux (0.007–0.925 m h^{-1}), and water level response (0.01–0.14 m) were observed. Results from this study helped to improve our understanding of the surface water and shallow groundwater interactions in an irrigated valley in northern New Mexico. The field data set obtained in this study can benefit future model characterization and contribute to extrapolating local results to larger spatial areas.

The increase in water demand compared with supply in the southwestern United States requires careful use of the water resources available. At the same time, it also requires a better understanding of the physical mechanisms involved in the replenishment of local and regional aquifers. Increases in human population near water sources, such as lakes and streams, increase water extraction, and the associated change in land use puts additional pressure on local aquifers and their mechanisms of recharge. Therefore, it is essential to have a better understanding of the hydrologic mechanisms responsible for the replenishment of the aquifers, especially those processes related to soil water fluxes, deep drainage, and aquifer recharge (Seyfried et al., 2005).

Water infiltration into the soil affects several aspects of soil management, such as water storage in the root zone, transport of fertilizers to the roots, and microbial and biochemical transformations of nutrients and organic matter. Soil water is critical in regulating the water and heat energy exchange between soils, plants, and the atmosphere and plays an important role in many hydrologic, biological, and biogeochemical processes (Lal and Shukla, 2004). In arid environments, a significant amount of recharge to shallow aquifers comes from stream losses (Wilcox et al., 2007) and from irrigation water infiltration in agriculture corridors (Fernald et al., 2007; Ochoa et al., 2007; Schoups et al., 2005; Willis and Black, 1996). Surface irrigation (e.g., border irrigation) has the potential to contribute to aquifer recharge, depending on the soil physical properties and the amount of water applied. Water recharge from surface irrigation becomes more evident in small-sized basins with narrow floodplains, where permeable alluvium allows deep percolation and subsurface flow, which causes groundwater recharge and return flow. This kind of scenario is typically found in northern New Mexico, where irrigated valleys with alluvial soils are commonly found along the Rio Grande. In these agriculture corridors, surface irrigation often exceeds plant consumptive demand and excess irrigation percolates below the root zone and ultimately joins the shallow aquifer (Ochoa et al., 2007).

Several methods have traditionally been used for investigating the process of soil water and groundwater recharge interactions (de Vries and Simmers, 2002; Scanlon et al., 2003; Sophocleous, 2001). Some of these methods involve calculation of infiltration rates based on crop-irrigation deep percolation (Jaber et al., 2006; Sammis et al., 1982), measurements of water transmission losses (Fox et al., 2004; Hunt et al., 2001; Vazquez-Suñe et al., 2007), changes in the groundwater level (Healy and Cook, 2002; Sanford, 2002; Sophocleous, 1991), and the use of isotopes to reveal water hydrochemical interactions (Flint et al., 2002;

C.G. Ochoa and A.G. Fernald, Dep. of Animal and Range Sciences, New Mexico State Univ., PO Box 30003, MSC 3I, Las Cruces, NM 88003; S.J. Guldan, Alcalde Sustainable Agriculture Science Center, PO Box 159, Alcalde, NM 87511; and M.K. Shukla, Dep. of Plant and Environmental Sciences, New Mexico State Univ., PO Box 30001, Las Cruces, NM 88003. Received 7 Mar. 2008. *Corresponding author (carochoa@nmsu.edu).

Vadose Zone J. 8:414–425
doi:10.2136/vzj2008.0059

Stonestrom et al., 2003). These methods, however, are based on observations made either in the upper soil layer, in the root zone, or in the water table, ignoring the rest of the vadose zone as the intermediate area of regulation and transport of infiltration water. In this study, direct measurements were used to assess water transport through the entire vadose zone and the water level response to surface irrigation. The objective of the study was to characterize water movement through the shallow vadose zone in three different soils following surface irrigation. Assessing water movement through the soil surface–vadose zone–aquifer continuum is a relevant step for calculating and simulating the soil water budget and aquifer recharge rate of an irrigated valley in northern New Mexico.

Materials and Methods

Study Site and Experimental Design

This study was conducted at New Mexico State University's Alcalde Sustainable Agriculture Science Center, 8 km north of Española, NM. The Alcalde Science Center is located in the agriculture corridor between the Alcalde main irrigation ditch and the Rio Grande in the northern part of the Española basin, in the Velarde sub basin. Three soil types, Fruitland sandy loam (a coarse-loamy, mixed, superactive, calcareous, mesic Typic Torriorthent), Werlog clay loam (a fine-loamy, mixed, active, calcareous, mesic Aquic Ustifluvent), and Abiquiu-Peralta complex (a sandy-skeletal, mixed, mesic–coarse-loamy, mixed, superactive, calcareous, mesic Typic Ustifluvent) (Soil Survey Staff, 2008), dominate the landscape and account for 85% of the irrigated land of the agriculture corridor along the Alcalde ditch. These three soils are present in the Alcalde Science Center and can be described by their proximity to the river or the ditch. The Abiquiu-Peralta complex soil is found near the river, the Werlog clay loam is located near the middle of the corridor, and the Fruitland sandy loam soil is between the middle of the field and the Alcalde ditch. The Alcalde Science Center has 24 ha of irrigated land for research on various forage, fruit, vegetable, and alternative high-value crops using primarily border or furrow irrigation, by far the most common practice in the valley and region. The study site is located at an elevation of 1733 m. For the period of record 1953–2006, the average annual precipitation for the study site was 251 mm. Most precipitation occurs as rainfall during the summer season (102.3 mm). The average maximum annual temperature is 20.1°C, and the average minimum annual temperature is 1.1°C. Normally, the maximum temperature occurs during the month of July and the minimum temperature occurs during the month of January (Western Regional Climate Center, 2006).

The study site overlies a shallow unconfined aquifer; measured at the lowest level before the irrigation season that ran from April to November of 2007, the depth to the water table ranged from 1.5 to 4.1 m depending on proximity to the river. The regional flow is mostly influenced by the Rio Grande. Also, important tributaries coming from the Sangre de Cristo Range in the east side of the basin are Rio de Truchas and Cañada de Las Entrañas, which drain in the vicinity of the Truchas Peaks (Daniel B. Stephen and Associates, 2003). The shallow groundwater flow at the study site is influenced by the Alcalde ditch and crop-field deep percolation contributions (Fernald et al., 2007; Ochoa et al., 2007). During the winter when no water is flowing in the ditch, the flow paths follow the flow of the river (north to south) and during the irrigation season (April–November) when there is water flowing in the ditch, the flow paths orient more toward the river (Fernald and Guldan, 2006). A shallow groundwater gradient of 0.2% was obtained based on water levels measured in different experimental wells existing at the Alcalde Science Center.

In each of the three soil types, two 12- by 12-m experimental plots were installed. Plots 1 and 2 were installed in the Fruitland sandy loam soil; Plots 3 and 4 were installed in the Werlog clay loam soil; and Plots 5 and 6 were installed in the Abiquiu-Peralta complex soil. Plots 1 and 2 were installed 78 m apart from each other. Plots 3 and 4 were located 76 m apart from each other and 131 and 147 m to the west of Plots 1 and 2, respectively. Plots 5 and 6 were located 145 m apart from each other. Plot 5 was installed 134 m west of Plot 3 and Plot 6 was installed 120 m west of Plot 4 (Fig. 1). Test pits (1.2 m wide by 1.6 m long with variable depth to the water table) were excavated outside of each plot, adjacent to the north edge, for soil characterization and installation of soil water sensors. In addition, experimental wells were installed outside and within 1 to 2 m of the north and west sides of all plots and in the centers of Plots 1, 4, and 6. The schematic

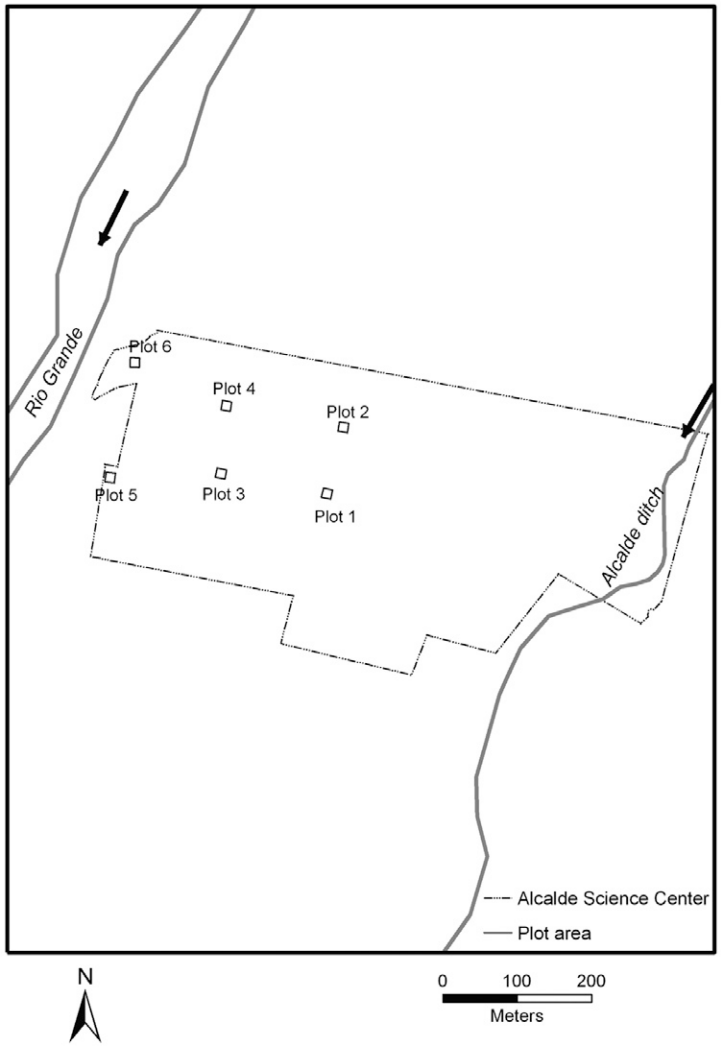

FIG. 1. Layout of experimental plots at the study site.

of a plot layout is presented in Fig. 2. After instrumentation, plots were bordered with an earthen berm about 0.6 m high.

Weather Data

Precipitation and air temperature data were obtained from a National Weather Service weather station located at the Alcalde Science Center. Pan evaporation was measured in the field 10 m south of Plot 1 using a 19-L plastic evaporation pan initially filled with 10 L of water. The water level change measured on a ruler in the water was recorded daily beginning on the day of each irrigation event and continuing an additional 2 to 5 d.

Soil Physical Properties

One test pit was excavated in each plot and layers of the soil profile were obtained based on soil morphological horizons. Plot 1 was characterized by a multilayered profile starting with a sandy clay layer in the upper 0.4 m, followed by sandy loam and sandy clay loam layers. A clay loam layer was found between 1.4 and 1.8 m, followed by sandy clay loam and sandy loam layers. The sand and gravel layer began at about 3 m deep, and the water table was reached at 4 m deep. Plot 2 showed a more uniform sandy loam layer to a depth of 1.8 m, followed by loam, sandy clay loam, and clay loam layers until the sand and gravel layer was reached at 3.3 m deep; the water table was reached at 4.1 m (Fig. 3). Plots 3 and 4 showed similar soil texture characterized by a sandy clay loam layer all the way down to 1.6 m, except that a clay loam layer between 0.5- and 0.8-m depth was found in Plot 4, and the water table was found at 2.9 m deep in Plot 3 and 2.8 m deep in Plot 4 (Fig. 4). Plot 5 showed a silty clay loam layer down to 0.5 m, followed by loamy soil, which extended to 1.3 m where the sand and gravel layer was found, and the water table was reached at 1.5 m deep. Plot 6 was characterized by a sandy loam soil in the upper 1.1 m followed by the sand and gravel layer; the water table was reached at 2.5 m deep (Fig. 5).

Soil samples for determining bulk density, ρ_b, and soil texture were collected from the test pits in the wall opposite the one where sensors were installed in each plot, starting at the 0.1-m depth from the soil surface and from that point down every 0.5 m until the sand and gravel layer was reached (Fig. 6). Three soil samples for ρ_b were collected from these depths using a core soil sampler with 50-mm-diameter by 30-mm-length cylinders. The procedure proposed by Blake and Hartge (1986) was used to calculate ρ_b. One 50-g soil sample was collected at each depth for determining soil texture using the hydrometer method (Gee and Bauder, 1986). Additionally, soil samples were collected at each soil depth for calibrating the soil water sensors. Samples were taken from the same wall opposite to the one where sensors were installed in Plots 1, 3, and 6 and at the same depth increment as for the ρ_b and soil texture samples. A soil volume of about 6 L with an approximate weight ranging from 4 to 5 kg was collected. These soil samples were air dried for at least 48 h and sieved through a 2-mm sieve.

Soil Water Instrumentation

A vertical nest of soil water content sensors (Model CS616, Campbell Scientific, Logan, UT) was installed in the test pit south

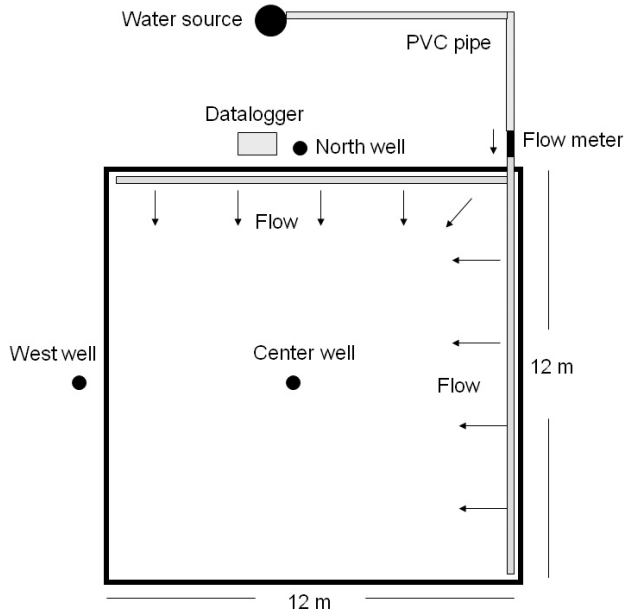

FIG. 2. Schematic of wells and instrumentation installed in the experimental plots, showing water source and flow direction.

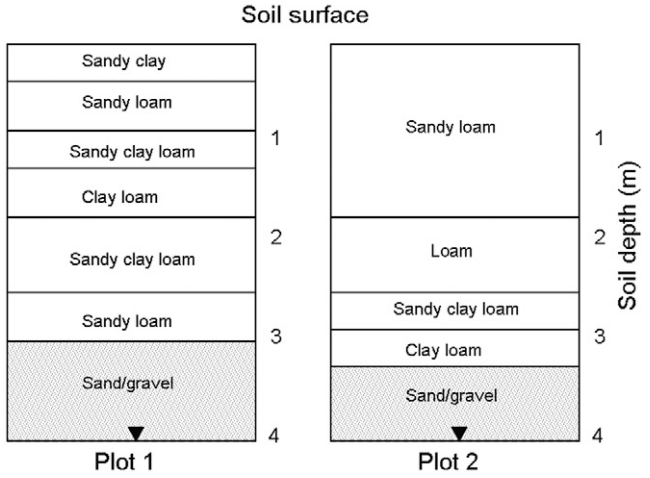

FIG. 3. Soil profile characterization based on soil morphological horizons and soil texture analysis in the Fruitland sandy loam soil, Plots 1 and 2.

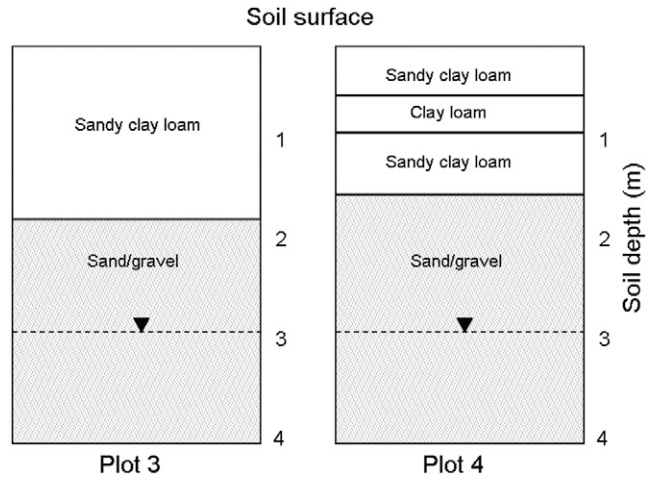

FIG. 4. Soil profile characterization based on soil morphological horizons and soil texture analysis in the Werlog clay loam soil, Plots 3 and 4.

wall (see Fig. 6). In all plots, soil water sensors were installed at the same depths where bulk density and texture samples were collected. The nest of sensors continued down as near as possible to the water table, at the same 0.5-m depth increments. Soil water sensors were installed horizontally so that the 0.3-m length of the sensor waveguide was inserted into the plot area.

Before field installation, the soil water sensors were tested in the lab for differences in measuring soil volumetric water content. All sensors were submerged in tap water and measurements were recorded for 10 min at 1-min intervals. Sensors were subsequently suspended in air and 10 more measurements were recorded following the same routine. Because no significant differences in measured soil volumetric water contents were observed between sensors, two soil water sensors were randomly selected for further soil volumetric water content calibration based on soil properties. Soil from each 6-L sample was packed in a clear acrylic column (90 mm wide by 140 mm long by 400 mm high) to a depth of 350 mm. One soil water content probe was inserted in the soil column and attached to a datalogger. A laptop computer was connected to the datalogger programmed to allow real-time data collection of the output period, OP, value used in the calibration for water content (Campbell Scientific, 2006). A volume of 200 mL of water was applied at the top of the soil column and allowed to infiltrate entirely into the soil. The OP and wetting front depth were recorded immediately after the water had completely infiltrated into the soil. This process was repeated until saturation was reached. The soil column was weighed before water additions and at saturation. The bulk density in the soil column, ρ_{b_column}, was calculated as the ratio of dry soil weight to dry soil volume. Soil gravimetric water content, w_{column}, was calculated as the difference between the wet soil weight and dry soil weight divided by the dry soil weight (Gardner, 1986). Then w_{column} values were multiplied by the soil ρ_{b_column} to obtain the volumetric water content in the column:

$$\theta_{column} = w_{column}\rho_{b\_column} \quad [1]$$

The θ_{column} was plotted against OP to obtain a specific calibration equation for calculating the soil volumetric water content in soil layers with similar texture.

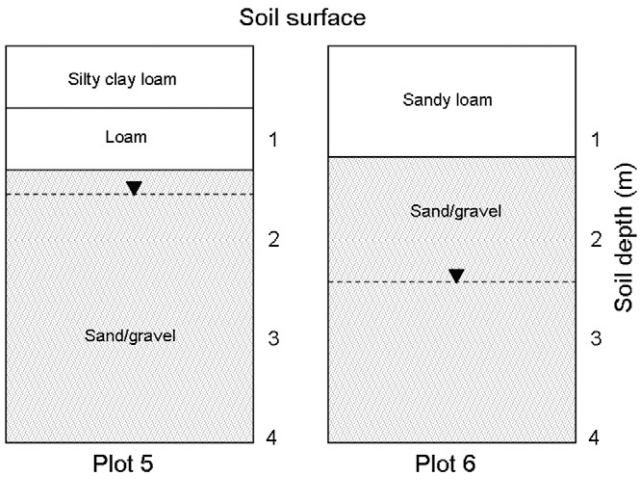

FIG. 5. Soil profile characterization based on soil morphological horizons and soil texture analysis in the Abiquiu-Peralta complex soil, Plots 5 and 6.

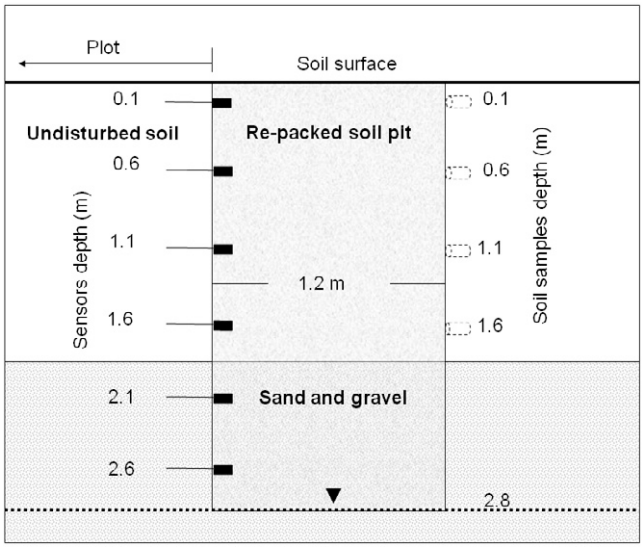

FIG. 6. Schematic of soil water sensor installation and soil sample collection in Plot 4.

Soil Preparation and Irrigation

The soil surface in all plots was leveled as much as possible using a blade attached to a tractor, then a rototiller was used to loosen the topsoil layer. The soil was also rototilled on 10 July 2007 for weed control and on 25 July 2007 before planting winter wheat (*Triticum aestivum* L.) in each plot. A slope of ≤0.5%, oriented from northeast to southwest, was observed after leveling and rototilling practices were applied in all plots.

Several surface (border) irrigations were applied on bare soil and on vegetated soil, after winter wheat emerged, in each plot. Gravity-fed and pumped irrigation discharge was approximately 320 L min^{-1}. To be certain that water reached the area where the soil water sensors were located and to enhance irrigation uniformity, two polyvinyl chloride (PVC) irrigation pipes of 50-mm diameter, perforated every 0.6 m, were installed along two plot boundaries (see Fig. 2). These pipelines formed an L shape that was connected to the supply pipe.

A total of eight border irrigations ranging from 110 to 380 mm were applied to each plot. A graduated scale marked with 25-mm increments was placed in all plots and the stage was visually observed and recorded at variable intervals during some irrigation events. During a final irrigation in Plot 1, a pressure transducer was installed on the soil surface to measure the water stage every 10 min for validation of visual observations. Close agreement between measured and visually observed values was noted. The total volume of water applied for a particular irrigation event, V (m^3), was measured using an insertion paddle-wheel flow meter (Model PF-P-80-40-2.0 with totalizer, Keeton Industries, Wellington, CO) mounted in a PVC pipe of 50-mm diameter. The depth of water applied, IRR (mm), was calculated based on the volume of water applied divided by the total area of the plot, A_{plot} (m^2). The flow meter was tested for volume accuracy by comparing volumes added to a 380-L stock tank to those volume values recorded by the flow meter totalizer. Results showed a 1 to 2% difference in measurements, which was considered accurate enough for the purposes of this study.

Changes in Soil Water Content

Volumetric soil water content, θ, was recorded every minute before and through approximately 24 h after the start of irrigation, and every hour thereafter. The change in volumetric soil water content, Δθ, at each soil water sensor depth was calculated as the difference between the average initial soil water content, $\theta_{initial}$, before irrigation and the average soil water content measured 24 h after the start of irrigation, $\theta_{24h.}$ The peak soil water content, θ_{peak}, observed within the 24-h period following the start of irrigation was also recorded. Values for $\theta_{initial}$, θ_{peak}, θ_{24h}, and Δθ were also averaged across the soil profile in each plot. For that purpose, the soil profile was considered to be the fine-textured portion of the alluvium soil, without including the sand and gravel layer in Plots 1, 3, 4, 5, and 6 or the coarse sand layer in Plot 2.

Water Transport Velocity, Water Flux, and Infiltration

Soil water content data were used to determine the time of arrival, t (h), of the wetting front to each sensor depth. The wetting front time of arrival was denoted as the first indication of increase in volumetric soil water content measured in each soil water sensor following an irrigation application. The changes in soil volumetric water content and the velocity of propagation of the wetting front, v (m h^{-1}), can be used for calculating the water flux, q (m h^{-1}), throughout the unsaturated zone (Dahan et al., 2007). The water flux moving through the soil profile was calculated using $q = v\,\Delta\theta$.

Cumulative infiltration, Z, and infiltration rates, I, in each plot during and after irrigation were calculated based on stage measurements. Two cumulative infiltration values were calculated. The first value was calculated at the time of cutoff, Z_{tco} (mm), and the second value was calculated 24 h after the onset of irrigation, Z_{24h} (mm). The Z_{tco} value was obtained by subtracting the water stage measured at the time of cutoff from the calculated IRR. The Z_{24h} value was obtained by subtracting the stage measurement observed at the 24-h mark after the onset of irrigation from the water stage observed at the time of cutoff. The total amount of water infiltrated at the 24-h mark, Z_{total} (mm), following irrigation was obtained by the sum of Z_{tco} and Z_{24h} minus the measured evaporation for the day. Two infiltration rates were calculated, the first infiltration rate was calculated during the time of irrigation, I_{irr} (mm h^{-1}), and the second was calculated 24 h after the onset of irrigation I_{24h} (mm h^{-1}). The I_{irr} was obtained by dividing the amount of water infiltrated at the time of cutoff by the number of hours that the irrigation lasted. The I_{24h} value was calculated by dividing the amount of water infiltrated between the time of cutoff and the 24-h mark after the onset of irrigation by the number of hours between these two times.

Shallow Aquifer Water Level Response

Two to three driven-point wells with a galvanized pipe of 50-mm diameter and a bottom screen of 1.2-m length were installed in each plot. Three wells were installed in Plots 1 and 4: one well was installed in the center of the plot, and the other two wells were installed on the north and west outside of each plot. Two wells were installed in Plots 2, 4, 5, and 6, in the north and west outside of each plot. All wells located outside the plots were within 1.2 m of the plot border. At installation, all wells were submerged at least 0.3 m below the water table. A well previously installed near the center of Plot 6 was also used for collecting water level data. This PVC (50-mm-diameter) well was 7.6 m deep with a 1.5-m solid pipe riser above a machine-slotted well screen extending from the riser down to 3 m below the water table at the time of installation in winter. All wells were geopositioned using a global positioning system unit (Model Pro XRS, Trimble Navigation, Ltd., Sunnyvale, CA) and were surveyed for elevation using a total station (Model GTS 226, Topcon Positioning Systems, Pleasanton, CA). All wells in Plots 1, 2, 3, 5, and 6 were equipped with stand-alone pressure transducers (Model U20-001-01, Onset Computer Corp., Bourne, MA) for measuring the water level. Also, the three wells installed in Plot 4 were equipped with pressure transducers (Model PDCR 1830-8388, Campbell Scientific, Inc., Logan, UT) attached to a datalogger for measuring the water level. All pressure transducers were programmed to collect water level data every 3 min during the entire irrigation season. The water level data collected were used to characterize water level fluctuations during specific irrigation events and throughout the entire irrigation season.

Results and Discussion

Weather Data Results

During the time of the experiment (May–November), rainfall totaled 166.4 mm. Monthly rainfall averaged 27.7 mm. August had the most rainfall, with 42.7 mm, and October had the least, with 5.3 mm. No precipitation occurred during any of the water application dates. The maximum temperature during the time of the experiment was recorded on 3 July 2007 at 36.7°C. The minimum temperature of –4.4°C was recorded on 2 Nov. 2007. Evaporation rates measured during the dates of water application ranged from 3 to 12 mm. The highest evaporation rate (12 mm) was observed on 11 July 2007, on which date the temperature reached 35°C. The lowest evaporation rate (3 mm) was recorded on 2 Nov. 2007 when the maximum temperature reached 20.6°C.

Soil Properties

Soil physical properties obtained from soil samples collected were different across soil types but were also different across plots. The textural composition for the Fruitland sandy loam soil in Plot 1 was characterized by a high clay content in the upper 0.1-m layer and by a restrictive layer of clay loam soil at a depth of 1.6 m that slowed the percolation of irrigation water (Table 1). The Fruitland sandy loam soil in Plot 2 showed a more uniform sandy loam texture in the upper 1.6 m, followed by a higher clay content in the lower part of the soil profile before the coarse sand layer was reached. The textural composition of the Werlog clay loam soil in Plots 3 and 4 was less varied, and most soil samples showed a sandy clay loam soil texture. The samples collected at the 0.6-m soil depth in Plot 4 showed a higher content of silt and clay than the other soil samples in both plots. The textural composition of the Abiquiu-Peralta complex soil was different between Plots 5 and 6. High contents of silt and clay were observed in the upper layer of Plot 5, followed by a layer of high sand and silt content. Plot 6 showed a uniform layer of sandy loam texture in the top 1.1 m above the sand and gravel layer. Soil bulk density ranged from 1.27 to 1.63 Mg m^{-3} in the Fruitland sandy loam soil, from 1.18

Table 1. Bulk density and textural composition of the three soil types being evaluated.

Plot	Soil depth	Bulk density	Sand	Silt	Clay
	m	Mg m^{-3}		%	
		Fruitland sandy loam soil			
1	0.1	1.53 ± 0.06†	56.8	2.8	40.4
1	0.6	1.52 ± 0.05	68.8	14.8	16.4
1	1.1	1.63 ± 0.02	54.8	18.8	26.4
1	1.6	1.46 ± 0.07	20.5	46.5	33.0
1	2.1	1.52 ± 0.05	62.5	12.5	25.0
1	2.6	1.36 ± 0.04	74.5	6.5	19.0
1	>3.0	–	–	–	–
2	0.1	1.54 ± 0.06	63.28	22.2	14.52
2	0.6	1.51 ± 0.03	71.28	15.2	13.52
2	1.1	1.45 ± 0.05	61.2	19.2	19.6
2	1.6	1.53 ± 0.02	63.2	20.2	16.6
2	2.1	1.35 ± 0.04	39.16	35.2	25.64
2	2.6	1.44 ± 0.02	47.2	22.2	30.6
2	3.1	1.27 ± 0.02	40.92	30.12	28.96
2	>3.3	–	–	–	–
		Werlog clay loam soil			
3	0.1	1.60 ± 0.02	58.8	10.8	30.4
3	0.6	1.39 ± 0.02	52.8	14.8	32.4
3	1.1	1.27 ± 0.02	62.8	6.8	30.4
3	1.6	1.18 ± 0.02	72.5	2.5	25.0
3	>1.8	–	–	–	–
4	0.1	1.60 ± 0.02	57.1	15.1	27.8
4	0.6	1.44 ± 0.04	27.0	39.0	34.1
4	1.1	1.34 ± 0.02	67.0	7.0	26.1
4	1.6	1.18 ± 0.03	62.9	9.0	28.1
4	>1.6	–	–	–	–
		Abiquiu-Peralta complex soil			
5	0.1	1.32 ± 0.02	19.2	43.2	37.7
5	0.6	1.46 ± 0.05	49.2	33.2	17.6
5	> 1.3	–	–	–	–
6	0.1	1.62 ± 0.03	76.8	6.8	16.4
6	0.6	1.60 ± 0.02	78.8	4.8	16.4
6	>1.1	–	–	–	–

† Mean ± standard deviation.

to 1.60 Mg m^{-3} in the Werlog clay loam soil, and from 1.32 to 1.62 Mg m^{-3} in the Abiquiu-Peralta complex soil (Table 1).

Changes in Soil Water Content

Soil water content varied across depths in all plots (Table 2), with Plot 1 having high soil water content at the 1.6-m depth where the soil texture was clay loam (see Table 1). In Plot 2, high values were observed at 2.1 and 2.6 m for all soil water parameters evaluated. Plot 5 had the lowest initial soil water content in all depths when compared with the rest of the plots. The Fruitland sandy loam soil Plots 1 and 2 showed the smallest variation in $\Delta\theta$ (0.03 m^3 m^{-3}) for the entire soil profile (Table 2). Soil water sensors located at 3.6 and 3.95 m in Plot 1 and at 3.6 and 4.1 m in Plot 2 were constantly saturated due to their locations near or under the water table. Therefore, increases in soil water were not observed during the time of the study. The Werlog clay loam soil, Plots 3 and 4, showed 0.05 and 0.09 m^3 m^{-3} changes, respectively, in soil water in the soil profile (Table 2). The Abiquiu-Peralta complex soil in Plot 5 showed the highest soil profile average $\Delta\theta$ of 0.09 m^3 m^{-3} (Table 2).

Wetting Front Arrival Time

The time of arrival of the wetting front, marked as the first indication of change in soil water content in each soil water sensor, varied across plots and sensor depths (Table 3). Low rates

Table 2. Changes in selected soil water parameters averaged across irrigations.

Sensor depth	Initial water content	Peak water content	Water content 24 h after onset of irrigation	Change in water content
m		m^3 m^{-3}		
		Plot 1		
0.1	0.316	0.385	0.352	0.035
0.6	0.235	0.288	0.255	0.021
1.1	0.345	0.42	0.412	0.067
1.6	0.452	0.487	0.486	0.034
2.1	0.22	0.263	0.241	0.021
2.6	0.314	0.324	0.32	0.007
3.1	–	–	–	–
Mean	0.313	0.361	0.344	0.031
		Plot 2		
0.1	0.224	0.328	0.311	0.087
0.6	0.222	0.344	0.325	0.103
1.1	0.292	0.365	0.341	0.049
1.6	0.392	0.414	0.406	0.014
2.1	0.455	0.459	0.459	0.004
2.6	0.417	0.42	0.419	0.002
3.1	0.323	0.324	0.322	−0.001
Mean	0.335	0.372	0.363	0.028
		Plot 3		
0.1	0.336	0.412	0.385	0.049
0.6	0.401	0.426	0.423	0.023
1.1	0.346	0.432	0.424	0.078
1.6	0.257	0.321	0.319	0.062
Mean	0.335	0.398	0.388	0.053
		Plot 4		
0.1	0.255	0.443	0.421	0.166
0.6	0.359	0.4	0.388	0.029
1.1	0.3	0.409	0.4	0.1
1.6	0.31	0.37	0.366	0.055
Mean	0.306	0.405	0.394	0.087
		Plot 5		
0.1	0.167	0.403	0.302	0.135
0.6	0.163	0.322	0.248	0.086
1.1	0.034	0.283	0.091	0.057
Mean	0.121	0.336	0.214	0.092
		Plot 6		
0.1	0.352	0.433	0.408	0.056
0.6	0.316	0.381	0.369	0.054
1.1	–	–	–	–
Mean	0.334	0.407	0.389	0.055

of wetting front propagation were observed in Plots 1 and 2. In Plot 1, soil water increases were observed in sensors located at or above the 1.1-m depth from the soil surface for all irrigations. The arrival time at the 1.1-m sensor depth varied from 1.4 h after the 220-mm irrigation to 16 h after one 110-mm irrigation. The wetting front did not reach the deeper sensors following most of the water applications; however, an increase in soil water was observed at the 3.1-m sensor depth 6.5 h after the first 380-mm irrigation applications (Fig. 7) and 5.3 h after the second 380-mm irrigation (Table 3). In Plot 2, more soil water increases were observed in deeper sensor locations than in Plot 1, and, similar to Plot 1, the wetting front reached a depth of 3.1 m only after an irrigation of 380 mm; however, it took 23.1 h for the wetting front to arrive at this sensor depth (Table 3). In Plots 3 and 4, increases in soil water content were observed in most of the soil water sensors, except in those sensors that were very close to or below the water table (Table 3). In Plot 4, similar soil water responses were observed following the 330- and 380-mm

Table 3. Time of arrival of the wetting front to different sensor depths following different irrigation depths ranging from 110 to 380 mm.

Sensor depth	Arrival time									
	110 mm	160 mm	220 mm	270 mm	110 mm	110 mm	160 mm	380 mm	330 mm	380 mm
m	h since onset of irrigation									
					Plot 1					
0.1	0.3	0.1	0.1	–	0.1	NA†	NA	0.6	0.3	1.1
0.6	3.8	1.4	1.2	–	0.9	NA	NA	2.0	1.4	2.6
1.1	6.0	5.8	1.4	–	4.4	16.0	9.1	2.6	2.2	2.8
1.6	–	–	4.6	–	8.8	–	–	2.7	–	3.1
2.1	–	–	–	–	–	–	–	2.7	–	3.6
2.6	–	–	–	–	–	–	–	3.3	–	4.0
3.1	–	–	–	–	–	–	–	6.5	–	5.3
3.6	–	–	–	–	–	–	–	–	–	–
4.0	–	–	–	–	–	–	–	–	–	–
					Plot 2					
0.1	0.6	0.4	0.5	0.1	0.4	1.2	0.6	0.1	0.03	–
0.6	1.5	1.9	5.0	4.7	6.3	6.5	4.8	4.7	4.7	–
1.1	5.4	5.3	9.0	14.8	16.5	17.5	15.4	8.4	12.9	–
1.6	9.9	6.7	NA	9.3	–	–	–	11.0	23.1	–
2.1	18.4	13.6	20.7	–	–	–	–	15.6	–	–
2.6	–	–	23.3	–	–	–	–	16.5	–	–
3.1	–	–	–	–	–	–	–	23.1	–	–
3.6	–	–	–	–	–	–	–	–	–	–
4.1	–	–	–	–	–	–	–	–	–	–
					Plot 3					
0.1	0.1	0.03	0.8	–	1.0	0.6	0.8	0.3	0.9	–
0.6	0.8	0.3	1.5	–	1.9	1.9	1.3	1.9	1.4	–
1.1	2.1	1.5	2.8	–	3.7	4.5	2.3	3.7	1.9	–
1.6	8.9	4.1	6.0	–	8.9	12.3	7.1	7.4	8.7	–
2.1	–	5.4	11.0	–	13.9	17.2	16.2	13.5	12.7	–
2.6	–	16.2	–	–	–	–	–	–	–	–
					Plot 4					
0.1	0.2	0.2	–	–	0.1	0.1	0.2	0.2	0.2	–
0.6	1.5	0.6	–	–	0.9	1.2	1.2	1.4	1.0	–
1.1	5.0	0.8	–	–	2.1	2.1	2.5	1.8	1.3	–
1.6	22.8	1.1	–	–	4.8	3.8	4.7	3.4	3.2	–
2.1	–	5.4	–	–	7.5	6.6	7.8	5.9	7.8	–
2.6	–	19.4	–	–	–	–	–	–	–	–
					Plot 5					
0.1	0.1	0.03	0.1	–	0.02	0.02	0.03	0.03	0.02	–
0.6	NA	0.4	0.6	–	0.8	0.2	0.8	0.8	0.1	–
1.1	0.4	0.6	0.9	–	0.9	0.6	1.1	1.3	0.7	–
1.6	0.9	1.1	1.2	–	1.6	0.7	1.6	1.4	1.1	–
					Plot 6					
0.1	0.4	0.1	0.1	–	0.1	0.02	0.02	0.03	0.02	–
0.6	0.8	0.4	0.3	–	0.4	0.2	0.1	0.3	0.05	–
1.1	5.1	2.1	5.0	–	1.7	8.9	4.0	4.2	5.2	–
1.6	–	2.9	12.3	–	4.2	21.0	5.8	4.9	7.2	–
2.1	–	–	–	–	–	–	9.4	–	–	–

† NA, not available.

irrigations (Fig. 8). In Plot 5, an increase in soil water content was observed in all sensors after all irrigations. In this plot, the three sensors located in the upper 1.1 m of the unsaturated zone responded relatively rapidly and the probe located at the 1.6-m depth showed a muted response (Fig. 9). We attributed this probe muted response to high antecedent soil water content at this depth due to close water table proximity. Regardless of irrigation depth, Plot 6 showed highly variable times of response ranging from 0.02 to 21 h (Table 3).

Wetting Front Travel Velocity

Since the velocity of the wetting front is dependent on the arrival time, the velocity at which increases in soil water were observed in each sensor depth was also variable across plots and across sensor depths (Table 4). Plot 1 showed the most uniform velocity, with an average of 0.52 m h^{-1}, ranging from 0.32 to 0.72 m h^{-1}. Plot 2 showed a greater velocity of 0.79 m h^{-1} for the upper 0.1-m sensor depth, followed by a significant reduction in wetting front transport velocity for the rest of the sensor depths, with an average velocity of 0.22 m h^{-1}. Plots 3 and 4 showed closer wetting front velocities; both plots were characterized by high velocities at depths at or below 1.1 m and by low velocities at the 2.6-m depth. Plot 5 showed the highest wetting front velocity of all plots, with a value of 3.75 m h^{-1}. The lowest velocity observed in Plot 5 was 1.44 m h^{-1}. Plot 6 also showed a high velocity of the wetting front at the 0.1- and 0.6-m sensor depths, but a significant reduction was observed at the deeper sensor depths (Table 4).

Water Flux

As expected, water flux was also variable across plots, depths, and irrigations (Table 5). In Plot 1, the soil water sensor at 1.6 m

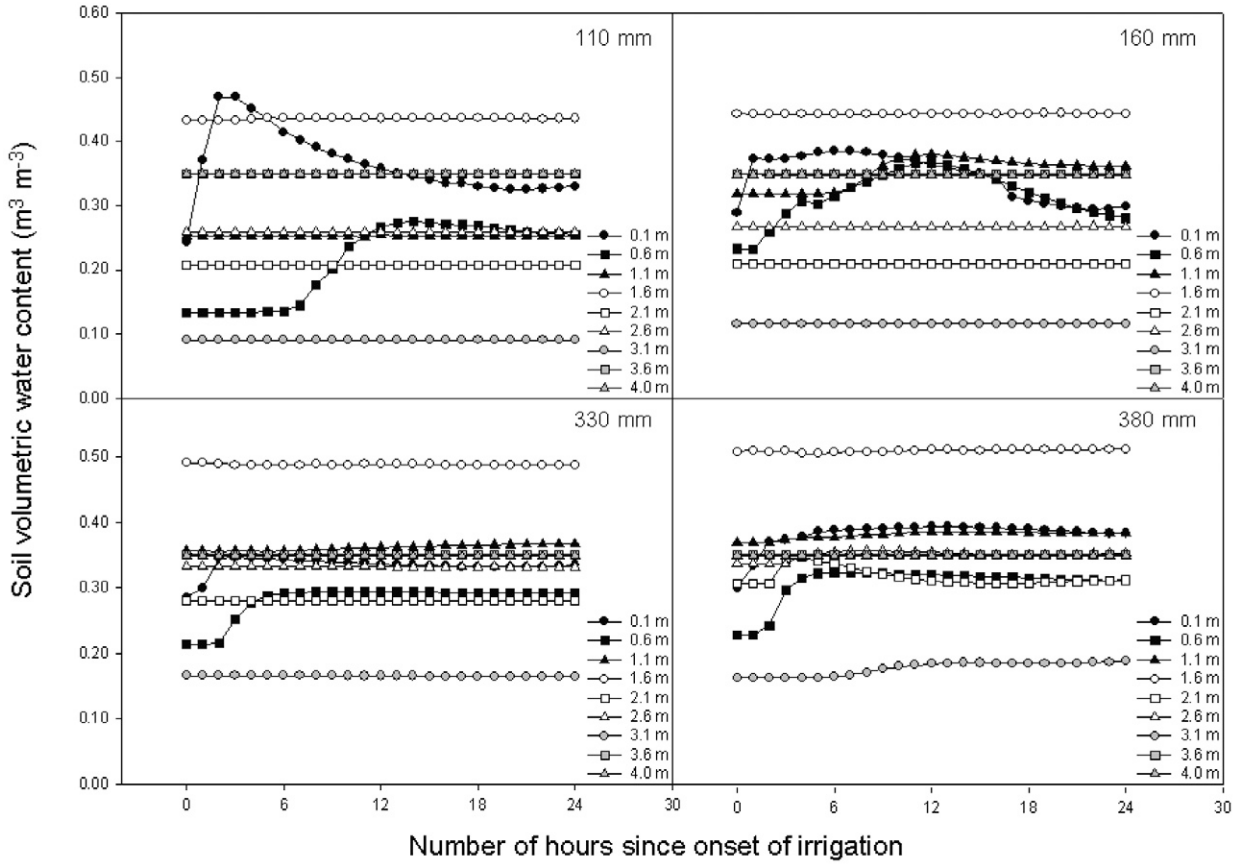

FIG. 7. Soil water sensor response to different irrigation depths (110, 160, 330, and 380 mm) in Plot 1, Fruitland sandy loam soil.

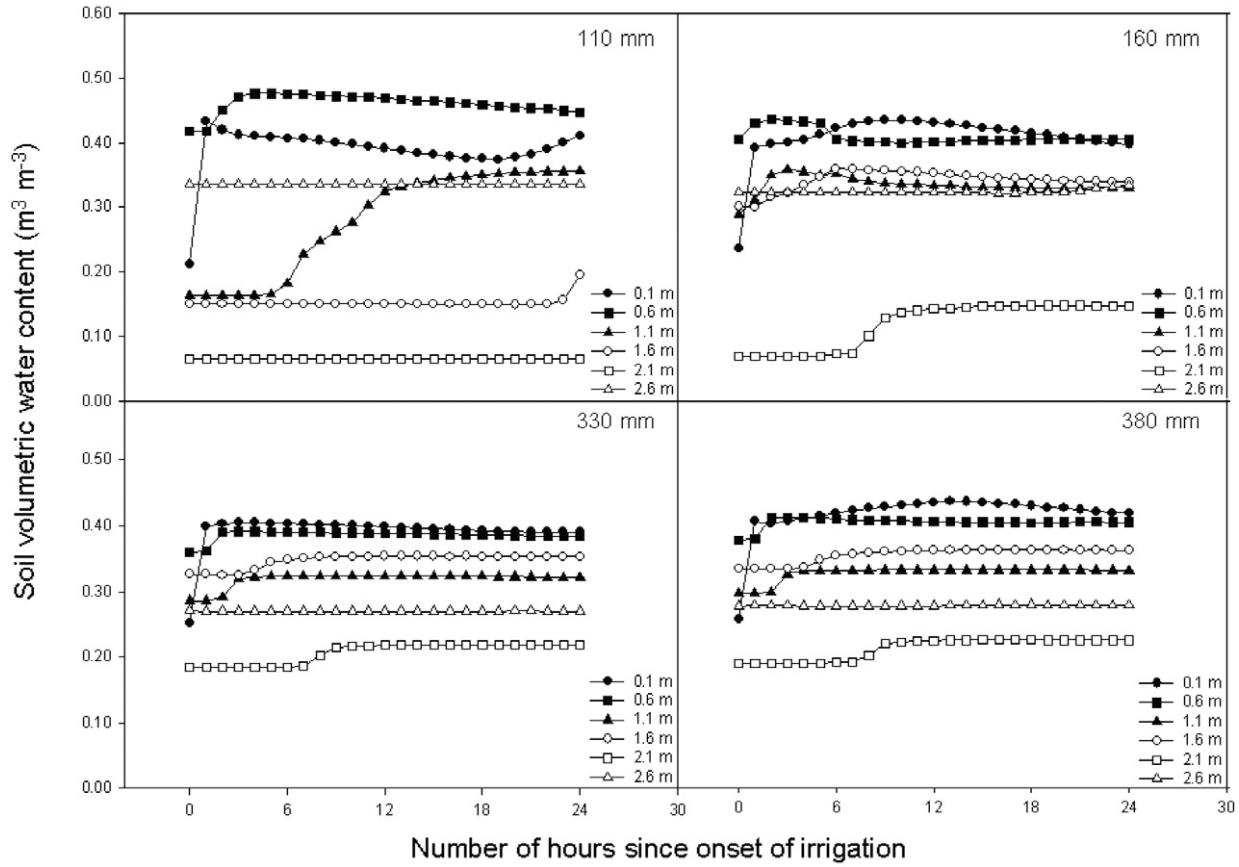

FIG. 8. Soil water sensor response to different irrigation depths (110, 160, 330, and 380 mm) in Plot 4, Werlog clay loam soil.

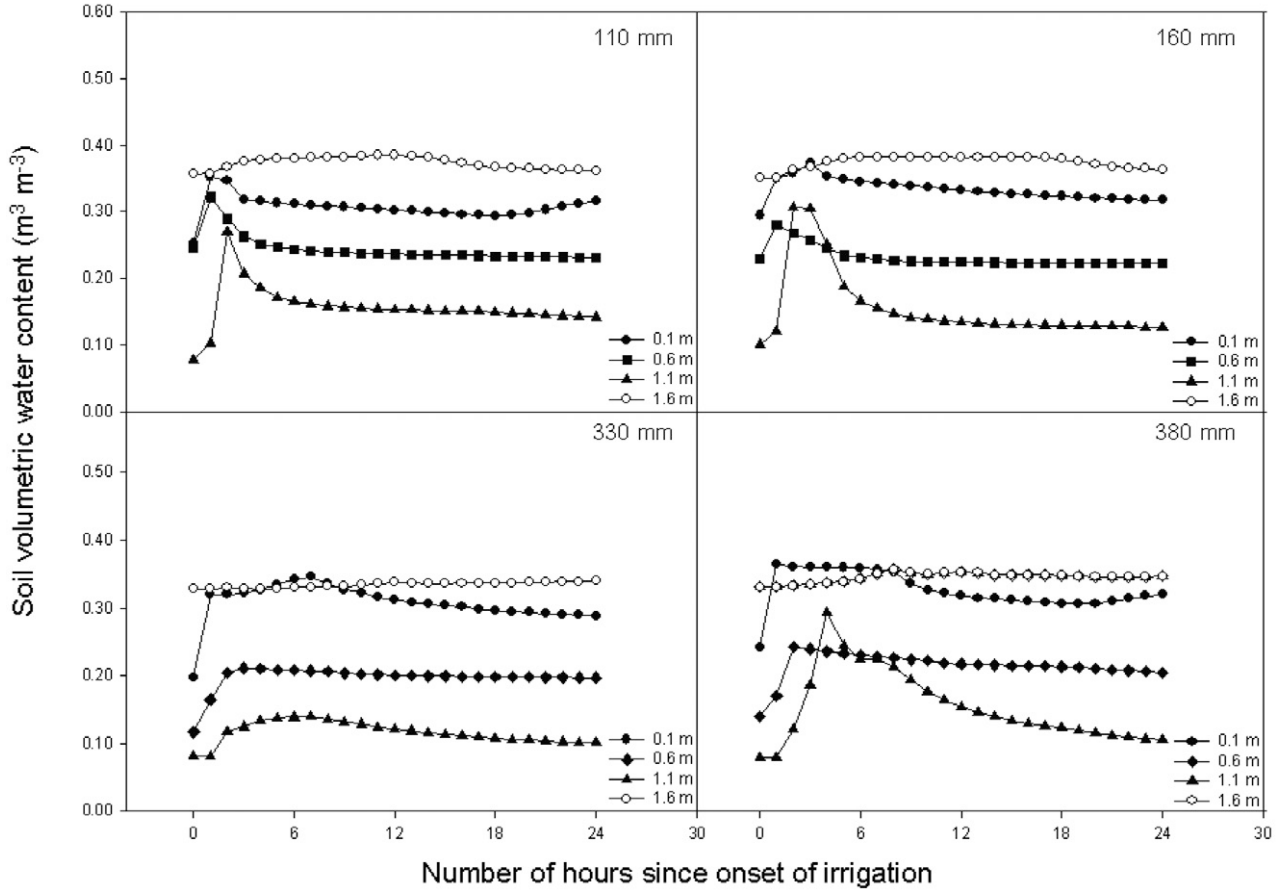

FIG. 9. Soil water sensor response to different irrigation depths (110, 160, 330, and 380 mm) in Plot 5, Abiquiu-Peralta soil.

showed a significant decrease in water flux. This was attributed to a clay loam layer located at that depth (see Table 1). In Plot 2, a significant decrease in water flux was observed at the sensors located at and below 2.1 m. This was attributed to the presence of a loamy soil layer that prevented a faster water flux. Plots 3 and 4 were characterized by high variability in water flux at different sensor depths. The smallest water flux was observed at the deepest sensor location for both plots. Plot 5 was characterized by a high water flux of 0.925 m h^{-1} at the upper 0.1-m sensor location and a low water flux of 0.027 m h^{-1} in the deepest 1.6-m sensor depth. Plot 6 showed relatively high water flux in the upper two sensor locations (0.1 and 0.6 m), followed by a significant drop in water flux for the 1.1- and 1.6-m sensor depths (Table 5).

Infiltration

In general, low to moderate levels of infiltration were observed, based on water stage measurements, in most plots (Table 6). The lowest levels of total infiltration, I_{total}, were observed in Plots 1 and 2 of the Fruitland sandy loam soil, where <30% of the total water applied infiltrated during the 24 h following irrigation. During and after irrigation, infiltration rates were generally similar for Plots 1 and 2 across different irrigation applications. Larger infiltration was observed in Plots 3 and 4 of the Werlog clay loam soil, where I_{total} ranged from 24 to 100% of the total water applied and I_{irr} and I_{24h} levels were moderately higher than those observed in Plots 1 and 2. The highest levels of infiltration were observed in Plots 5 and 6 of the Abiquiu-Peralta complex soil, particularly in Plot 5 where 100% of the water applied infiltrated within a few hours after application and

TABLE 4. Velocity of propagation of the wetting front averaged across irrigations.

Sensor depth	Average wetting front travel velocity					
	Plot 1	Plot 2	Plot 3	Plot 4	Plot 5	Plot 6
m	m h^{-1}					
0.1	0.59	0.79	0.60	0.69	3.75	2.98
0.6	0.39	0.17	0.62	0.59	2.25	3.25
1.1	0.32	0.12	0.45	0.65	1.50	0.31
1.6	0.41	0.12	0.22	0.52	1.44	0.28
2.1	0.68	0.10	0.19	0.31	–	–
2.6	0.72	0.13	0.16	0.13	–	–
3.1	0.53	0.13	–	–	–	–
Mean	0.520	0.223	0.373	0.482	2.235	1.705

TABLE 5. Water flux averaged across irrigations.

Sensor depth	Average water flux					
	Plot 1	Plot 2	Plot 3	Plot 4	Plot 5	Plot 6
m	m h^{-1}					
0.1	0.054	0.072	0.054	0.130	0.925	0.292
0.6	0.053	0.023	0.018	0.024	0.377	0.228
1.1	0.012	0.011	0.042	0.061	0.391	0.025
1.6	0.002	0.007	0.014	0.039	0.027	0.007
2.1	0.075	0.001	0.004	0.013	–	–
2.6	0.037	0.001	0.002	0.001	–	–
3.1	0.022	0.001	–	–	–	–
Mean	0.036	0.017	0.022	0.045	0.043	0.138

TABLE 6. Infiltration rates during and after water application and total infiltration for selected irrigations in 2007.

Plot	Date	Irrigation	During-irrigation infiltration rate	Post-irrigation infiltration rate	Total infiltration
		mm	mm h^{-1}		mm
1	11 July	110	7	1	34
	15 Aug.	110	7	1	31
	14 Sept.	380	20	5	120
	2 Nov.	380	23	5	120
2	10 July	110	5	1	23
	15 Aug.	110	2	1	22
	12 Sept.	380	15	4	95
3	11 July	110	21	3	102
	15 Aug.	110	7	7	112
	13 Sept.	380	56	5	158
4	11 July	110	20	2	68
	15 Aug.	110	13	1	38
	14 Sept.	380	17	7	177
5	11 July	110	45	62	110
	16 Aug.	110	88	60	110
	13 Sept.	380	124	76	380
6	11 July	110	3	3	83
	16 Aug.	110	4	2	52
	14 Sept.	380	9	9	221

I_{irr} was up to 0.124 m h^{-1}. In Plot 6, a range of 47 to 58% of IRR was infiltrated at the end of 24 h (Table 6). A surface layer of greater density and lower hydraulic conductivity, a product of constant tilling and water effects, is commonly found in layered cultivated soils (Smith et al., 2002). The low to moderate levels of infiltration observed in most plots were attributed to a combination of high levels of compaction made by the tractor wheels during the leveling and tilling practices and to an impervious, fine-textured layer observed on the surface of most plots. These observations are consistent with the findings of Dahan et al. (2007), who reported that a reduction in infiltration rate during their experiment was due to clogging of the pond bottom by fine particles and clay swelling. The high infiltration observed in Plot 5 was attributed to an extensive macropore flow system developed by the riparian vegetation located next to the plot. This macropore system was observed in this study during excavation of the pits for installing the wells and the sensors, when a very dense rooting system from Rio Grande cottonwood [*Populus deltoides* W. Bartram ex Marshall ssp. *wislizeni* (S. Watson) Eckenw.] trees with roots up to 8 cm in diameter were found (Fig. 10). These high rates of infiltration were similar to those reported by Meek et al. (1990), who found that an extensive taproot system and a well-developed macropore system in an alfalfa (*Medicago sativa* L.) field substantially increased the infiltration rate.

Water Level Response

According to Fernald and Guldan (2006), surface irrigation can alter the local shallow groundwater flow paths in the irrigated valley where this study took place. The water level response following surface irrigation was obtained based on water level fluctuations measured in the wells located in or near the different plots. To avoid interference from irrigation water applied to larger crop fields near the experimental plots, these larger fields were not irrigated for at least 4 d before and at least 3 d after irrigation of the plots. In addition, given the relatively small spatial and temporal resolution of the experiment, regional groundwater flow was considered

FIG. 10. Photo taken during the north-side well installation in Plot 5, showing a very dense rooting system beneath the surface of the plot.

negligible. The slow infiltration rates observed in most plots (see Table 6) resulted in minimal or no water level response following most irrigations. For example, in Plot 1, the water level response that can be attributed to plot irrigation occurred after the first 380-mm water application on 14 Sept. 2007, with a maximum rise of 40 mm observed in the west-side well 17 h after the end of irrigation (Fig. 11). The water level before the start of irrigation was about 3.6 m below ground level and it was observed that a significant water level rise started about 5 h after the end of irrigation. The three wells in Plot 1 showed the same time of response (see Fig. 11). In Plot 2, the water level response to irrigation behaved similarly to Plot 1 and it was only during the 380-mm irrigation that a water level rise observed in the wells could be attributed to irrigation. The 380-mm irrigation was applied on 12 Sept. 2007 and a maximum water level rise of 70 mm was observed in the west-side well of Plot 2 70 h after the end of irrigation. Wells at Plot 3 showed some water level response to irrigation for most of the irrigations applied, with a maximum water level rise of 80 mm observed after the 220-mm irrigation application on 27 June 2007. Interestingly, only a 20-mm water level rise was observed after the maximum irrigation application of 380 mm. Wells at Plot 4 showed a water level rise after four of the irrigation events. A 40-mm peak water level rise was observed 48 h after the first irrigation of 110 mm on 31 May 2007. Peak water level rises of 10 mm were noted 30 h after the end of the 110-mm irrigation on 11 July 2007 and 50 h after the 110-mm irrigation on 15 Aug. 2007. A 100-mm peak water level rise was observed in the north-side well 29 h after the 380-mm irrigation of 14 Sept. 2007.

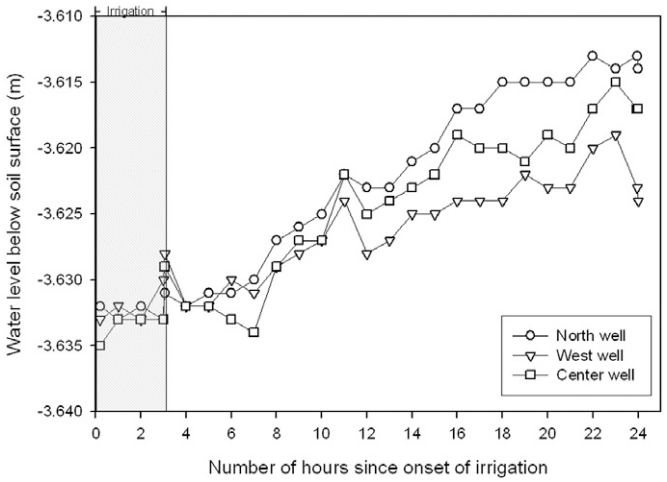

FIG. 11. Water level response measured at the three wells in Plot 1 following irrigation on 14 Sept. 2007.

A water level rise was observed following most irrigation applications in Plot 5; the peak water level rise ranged from 10 to 140 mm and the time to peak ranged from 1 to 6 h after the start of irrigation. The water level response was highly variable in the two wells installed at Plot 5 and can be observed in Fig. 12, where the west-side well presented a higher peak water level of 140 mm and a more rapid response of 1.2 h compared with the 60-mm peak water level and 2.5-h water level response in the north-side well for the 380-mm irrigation on 13 Sept. 2007. This was attributed to an uneven soil surface that created a ponding effect on the west side of the plot. The rapid infiltration observed in this plot was not reflected in water level rises as high as expected, however, given the amount and rate of infiltration following all irrigations; this was attributed to a rapid dissipation of the infiltrated water due to the proximity to an irrigation ditch and the river and to the extensive rooting system present in the area. In Plot 6, a water level response to irrigation was observed after all irrigation events. The maximum water level rise of 50 mm was measured after the 330-mm irrigation on 26 June 2007, with a time to peak water level of 17 h (data not shown). The water level response to surface irrigation measured in Plots 1 and 2 after different irrigation depths was significantly lower than the water level response measured in a related study conducted in a larger alfalfa field with a similar soil type and similar irrigation amounts (Ochoa et al., 2007).

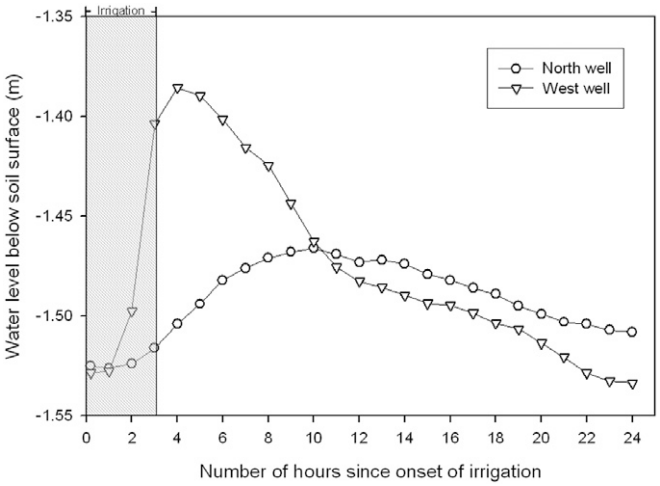

FIG. 12. Water level response measured at the two wells in Plot 5 following irrigation on 13 Sept. 2007.

Implications for Understanding and Management of Irrigation Water Percolation to Groundwater

The results of this study showed that irrigation water can be rapidly transported downward through Abiquiu-Peralta soil but not through Fruitland sandy loam or Werlog clay loam soils. In general, the water level response was found to be highly correlated to the amount of water applied, the permeability of the soil, and the depth to the water table. This study improves our understanding of the physical mechanisms involved in downward water movement and the shallow groundwater response to irrigation in three dominant soils of an irrigated valley in northern New Mexico. Some of the limitations of this study include the small size of the experimental plots and the farm machinery used in the experimental plots that may not entirely reflect prevailing farming and irrigation practices in the area. Important inferences can be made, however, to illustrate how surface irrigation can provide vertical input to shallow groundwater and return flow to the river, depending on soil physical properties and the amount of water applied. For instance, 57% of the total land of the 9-km^2 valley consists of Abiquiu-Peralta soil. The current farming practices in the valley include minimal or no chemical applications and most of the land is dedicated to agricultural purposes. Thus, there is a good potential for seasonal aquifer recharge and return flow from deep percolation of irrigation water.

Soil profile variability and the effects of this vertical variation on water infiltration and percolation have important implications for characterizing irrigation percolation and groundwater recharge. It has been shown that B horizon clay content is negatively correlated with a deep percolation rate (Willis and Black, 1996). From our detailed study results, it can be suggested that the lowest hydraulic conductivity found in high-clay-content layers limited deep percolation. These very low hydraulic conductivity layers were associated with longer times and smaller quantities of deep percolation.

Spatially uniform estimates of deep percolation and groundwater recharge in central California were improved by incorporating spatial variability in water balance components (Young and Wallender, 2002). We expect that incorporation of vertical variability into water balance estimates will improve these estimates. Methods to estimate irrigation return to groundwater have been extrapolated to the watershed scale (Dewandel et al., 2008) but do not include detailed characterizations of the fluvial valley soil complexities needed to accurately assess return flow. Interactions between surface water and groundwater have been studied for other areas (Lamontagne et al., 2005; Fernald et al., 2006), showing the importance of clay compared with gravel substrates for river and groundwater interaction rates. In locations where irrigation groundwater recharge becomes return flow to the river channel, understanding deep percolation through complex unsaturated-zone strata is vital for both surface water and groundwater management. An important ongoing research objective is to spatially characterize these vertical complexities to enable valley-scale modeling of deep percolation that becomes groundwater recharge and river return flow in these complex fluvial valley soils.

Further applications of the field data set obtained in this study include model characterization that will contribute to extrapolating local results to larger spatial areas.

Conclusions

The aim of this study was to characterize water movement through the soil surface–vadose zone–aquifer continuum in response to surface irrigation in three different alluvial soils of an irrigated corridor in northern New Mexico. The velocity of the wetting front and the water flux were relatively high in the Abiquiu-Peralta soil compared with the Fruitland sandy loam and Werlog clay loam soils; however, low infiltration rates were generally observed during and after water application in most plots. Low levels of infiltration found during the experiments were attributed to low hydraulic conductivity in the top soil layer. When irrigation water percolated into the aquifer, rises in shallow groundwater ranged from 10 to 140 mm. Results from this study contribute toward a better understanding of the surface water and shallow groundwater interactions in an irrigated valley of the Rio Grande in northern New Mexico.

Acknowledgments

We gratefully acknowledge the technical assistance of Val Archuleta, David Archuleta, David Salazar, Ciara Cusack, and Yeliz Cevik. This material is based on work supported by the New Mexico Agricultural Experiment Station and by the Cooperative State Research, Education and Extension Service, U.S. Department of Agriculture under Agreement no. 2005-34461-15661.

References

Blake, G.R., and K.H. Hartge. 1986. Bulk density. p. 363–375. *In* A. Klute (ed.) Methods of soil analysis. Part 1. Physical and mineralogical methods. 2nd ed. Agron. Monogr. 9. ASA and SSSA, Madison, WI.

Campbell Scientific. 2006. Instruction manual for CS616 and CS625 water content reflectometers. Campbell Scientific, Logan, UT.

Dahan, O., Y. Shani, Y. Enzel, Y. Yechieli, and A. Yakirevich. 2007. Direct measurements of floodwater infiltration into shallow alluvial aquifers. J. Hydrol. 344:157–170.

Daniel B. Stephen and Associates. 2003. Jemez y Sangre Regional Water Plan. Daniel B. Stephen and Associates, Albuquerque, NM.

de Vries, J.J., and I. Simmers. 2002. Groundwater recharge: An overview of processes and challenges. Hydrogeol. J. 10:5–17.

Dewandel, B., J.M. Gandolfi, D. de Condappa, and S. Ahmed. 2008. An efficient methodology for estimating irrigation return flow coefficients of irrigated crops at watershed and seasonal scale. Hydrol. Processes 22:1700–1712.

Fernald, A.G., T.T. Baker, and S.J. Guldan. 2007. Hydrologic, riparian, and agroecosystem functions of traditional acequia irrigation systems. J. Sustain. Agric. 30:147–171.

Fernald, A.G., and S.J. Guldan. 2006. Surface water–groundwater interactions between irrigation ditches, alluvial aquifers, and streams. Rev. Fish. Sci. 14:79–89.

Fernald, A.G., D.H. Landers, and P.J. Wigington, Jr. 2006. Water quality changes in hyporheic flow paths between a large gravel bed river and off-channel alcoves in Oregon, USA. River Res. Appl. 22:1–14.

Flint, A., L. Flint, E. Kwicklis, J. Fabrika-Martin, and G. Bodvarsson. 2002. Estimating recharge at Yucca Mountain, Nevada, USA: Comparison of methods. Hydrogeol. J. 10:180–204.

Fox, G.A., R. Malone, G.J. Sabbagh, and K. Rojas. 2004. Interrelationship of macropores and subsurface drainage for conservative tracer and pesticide transport. J. Environ. Qual. 33:2281–2289.

Gardner, W.H. 1986. Water content. p. 635–662. *In* A. Klute (ed.) Methods of Soil Analysis. Part 1. Physical and mineralogical methods. 2nd ed. Agron. Monogr. 9. ASA and SSSA, Madison, WI.

Gee, G.W., and J.W. Bauder. 1986. Particle-size analysis. p. 383–409. *In* A. Klute (ed.) Methods of soil analysis. Part 1. Physical and mineralogical methods. 2nd ed. Agron. Monogr. 9 ASA and SSSA, Madison, WI.

Healy, R.W., and P.G. Cook. 2002. Using groundwater levels to estimate recharge. Hydrogeol. J. 10:91–109.

Hunt, B., J. Weir, and B. Clausen. 2001. A stream depletion field experiment. Ground Water 39:283–289.

Jaber, F.H., S. Shukla, and S. Srivastava. 2006. Recharge, upflux and water table response for shallow water table conditions in southwest Florida. Hydrol. Processes 20:1895–1907.

Lal, R., and M. Shukla. 2004. Principles of soil physics. Marcel Dekker, New York.

Lamontagne, S., F.W. Learney, and A.L. Herczeg. 2005. Groundwater–surface water interactions in a large semi-arid floodplain: Implications for salinity management. Hydrol. Processes 19:3063–3080.

Meek, B.D.D., W.R. Rolph, D. Rechel, E.R. Carter, and L.M. Carter. 1990. Infiltration rate as affected by an alfalfa and no-till cotton cropping system. Soil Sci. Soc. Am. J. 54:505–508.

Ochoa, C.G., A.G. Fernald, S.J. Guldan, and M.K. Shukla. 2007. Deep percolation and its effects on shallow groundwater level rise following flood irrigation. Trans. ASABE 50:73–81.

Sammis, T.W., D.D. Evans, and A.W. Warrick. 1982. Comparison of methods to estimate deep percolation rates. J. Am. Water Resour. Assoc. 18:465–470.

Sanford, W. 2002. Recharge and groundwater models: An overview. Hydrogeol. J. 10:110–120.

Scanlon, B.R., A. Dutton, and M.A. Sophocleous. 2003. Groundwater recharge in Texas. Texas Water Dev. Board, Austin.

Schoups, G., C.L. Addams, and S.M. Gorelick. 2005. Multi-objective calibration of a surface water–groundwater flow model in an irrigated agricultural region: Yaqui Valley, Sonora, Mexico. Hydrol. Earth Syst. Discuss. 2:2061–2109.

Seyfried, M.S., S. Schwinning, M.A. Walvoord, W.T. Pockman, and B.D. Newman. 2005. Ecohydrological control of deep drainage in arid and semiarid regions. Ecology 86:277–287.

Smith, R.E., K.R.J. Smettem, P. Broadbridge, and D.A. Woolhiser. 2002. Applying infiltration models in layered soils and redistribution cases. p. 119–134. *In* Infiltration theory for hydrologic applications. Water Resour. Monogr. 15. Am. Geophys. Union, Washington, DC.

Soil Survey Staff. 2008. Official soil series descriptions. Available at ortho.ftw.nrcs.usda.gov/cgi-bin/osd/osdname.cgi (accessed 3 Jan. 2008; verified 19 Jan. 2009). USDA-NRCS Soil Surv. Div., Lincoln, NE.

Sophocleous, M.A. 1991. Combining the soil water balance and water level fluctuation methods to estimate natural groundwater recharge: Practical aspects. J. Hydrol. 124:229–241.

Sophocleous, M.A. 2001. Interactions between groundwater and surface water: The state of the science. Hydrogeol. J. 10:52–67.

Stonestrom, D.A., D.E. Prudic, R.J. Laczniak, K.C. Akstin, R.A. Boyd, and K.K. Henkelman. 2003. Estimates of deep percolation beneath native vegetation, irrigated fields, and the Amargosa-River channel, Amargosa Desert, Nye County, NV. Open-File Rep. 2003–104. USGS, Reston, VA.

Vazquez-Suñe, E., B. Capino, E. Abarca, and J. Carrera. 2007. Estimation of recharge from floods in disconnected stream–aquifer systems. Ground Water 45:579–589.

Western Regional Climate Center. 2006. Alcalde, New Mexico (290245). Period of record monthly climate summary. Period of record: 4/1/1953–12/31/2005. Available at www.wrcc.dri.edu/cgi-bin/cliMAIN.pl?nmalca (accessed 2 Feb. 2008; verified 19 Jan. 2009). WRCC, Reno, NV.

Wilcox, L.J., R.S. Bowman, and N.G. Shafike. 2007. Evaluation of the Rio Grande management alternatives using a surface-water/groundwater model. J. Am. Water Resour. Assoc. 43:1595–1603.

Willis, T.M., and A.S. Black. 1996. Irrigation increases groundwater recharge in the Macquarie Valley. Aust. J. Soil Res. 34:837–847.

Young, C.A., and W.W. Wallender. 2002. Spatially distributed irrigation hydrology: Water balance. Trans. ASAE 45:609–618.